Robust Linear Parameter-Varying Control for Safe and Effective Unstable Aircraft System Identification

Jeremy W. Hopwood[*] and Craig A. Woolsey[†]
Virginia Tech, Blacksburg, VA 24060

Large domain, accurate flight dynamic models with well-characterized uncertainty are often required for estimation and control of unmanned air vehicles. For unstable aircraft, identifying these models is a challenging task. Stabilizing controllers tend to suppress important dynamics, amplify artificial dynamics, and introduce correlation. For large domain model identification requiring large-amplitude excitation, there is often no stability guarantee, greatly increasing risk. To develop a model that covers the desired flight envelope, a two-phase data collection approach is taken where using a simple baseline controller, a set of linear, time-invariant models are identified about flight conditions that define the vertices of an uncertain polytopic linear parameter-varying (LPV) system. A robust LPV control law is then synthesized to stabilize the system with an H_∞ norm bound guarantee, allowing for excitation over a large domain for nonlinear system identification. This modeling approach is applied to a small quadrotor aircraft whose motion is robustly stabilized about a slowly varying reference velocity, which serves as the LPV scheduling parameter. The performance objective is chosen to allow sufficient excitation for nonlinear system identification while maintaining robust stability, thus allowing for higher-amplitude excitation signals to safely and effectively excite the aircraft dynamics over a large domain. The control law is demonstrated by simulating the LPV model identified from flight data.

I. Introduction

In many unmanned aircraft system (UAS) applications, large domain, accurate flight dynamic models are required for estimation and control. However, obtaining a finite-dimensional model that is valid across the entire flight envelope is a non-trivial task. For fixed-wing aircraft, the use of orthogonal phase-optimized multisine excitation signals (*multisines* for short) and multivariate orthogonal function (MOF) modeling have been successfully used to obtain global flight data and model structures, respectively [1, 2]. Note that in this paper, the term *global* refers to the feasible flight envelope as opposed to the full, mathematical state space. The use of multisines and MOF modeling works very well for statically stable aircraft that can be excited in an open-loop manner, i.e., without feedback stabilization. For unstable aircraft such as multirotor air vehicles, on the other hand, a nominal trajectory must be stabilized before actuator excitation can be applied. Therefore, an iterative approach is generally taken where each iteration involves data collection, model identification, control law design, and robustness analysis [3]. Part of the difficulty in this process stems from the fact that a stabilizing control law tends to introduce correlation, suppress dynamics of interest, and amplify artificial dynamics [4, Ch. 9]. More importantly, it is possible that input excitation signals used for model identification may drive the system outside the region of attraction of the locally stable reference motion. Here, we propose a methodology for obtaining uncorrelated large-domain excitation data while guaranteeing stability.

Identification of unstable aircraft can be done using either open-loop or closed-loop flight data. The former approach is only feasible, however, over time horizons that are short relative to the growth of the fastest unstable mode. This means global excitation data cannot be obtained in a continuous experiment. Having continuous, large-domain experimental data simplifies data collection and supports time-domain model identification methods such as output-error, filter-error, and Kalman filtering methods [4, 5]. To alleviate the practical issues associated with open-loop excitation, experimental data for unstable aircraft is typically obtained under stabilizing closed-loop control. Since we are interested in flight dynamic models for control and estimation purposes, we desire an open-loop model from closed-loop flight data. This is often done for linear model identification of multirotor aircraft [6]. However, in applications where the model must be applicable over a large domain (see [7], for instance), a nonlinear model must be identified. In this paper, we aim to concurrently design a controller and an excitation signal that allow for larger amplitude excitation suitable for

---

*Ph.D. Candidate, Crofton Department of Aerospace and Ocean Engineering, AIAA Student Member, jeremyhopwood@vt.edu
†Professor, Crofton Department of Aerospace and Ocean Engineering, AIAA Associate Fellow, cwoolsey@vt.edu

identifying large-domain nonlinear models. Larger excitations provide better signal-to-noise ratio (SNR), which is especially important in identifying flight dynamic models for small UAS [8]. Allowing for larger excitation is especially important for multirotor aircraft because they experience considerable vibration which tends to diminish the SNR. These observations further motivate the need to develop safe methods of performing large-amplitude identification maneuvers for unstable UAS.

This paper presents a methodology for obtaining global flight data for nonlinear model identification of unstable UAS. While we focus on the multirotor, the methods apply to unstable fixed-wing configurations as well as vertical takeoff and landing (VTOL) aircraft, including hybrid aircraft that transition between rotor-borne and wing-borne flight regimes. The approach we present involves two data collection phases of the system identification process as opposed to the traditional approach of incremental flight envelope expansions. First, linear time invariant (LTI) models are identified about a set of specific flight conditions, which are determined using a hypothesized model structure for the aerodynamic forces and moments. The identified models define a polytopic uncertain linear parameter-varying (LPV) system. Next, input excitation signals and a reference trajectory are concurrently designed along with a robust LPV control law that places a sub-optimal H_∞ norm bound on the map from input excitation to perturbation from the reference. Finally, this control law is used in the second phase of data collection in which the UAS is capable of fully-automated flights that span the desired flight domain in an efficient and safe manner for obtaining informative, uncorrelated data for nonlinear model identification.

The paper is organized as follows. Section II introduces the small quadrotor aircraft used to demonstrate the proposed modeling approach and covers the nonlinear rigid-body aircraft dynamics and how they are used to inform the LPV model derived in Section III. The initial model identification process is detailed in Section IV, which involves the first phase of data collection in the proposed methodology. Section V covers the development of excitation and reference signals along with the formulation of the H_∞ performance measure. The robust control design and closed-loop analysis is presented in Section VI. Finally, Section VII presents simulation results for the automated system identification flight experiment – the second and final phase of flight data collection.

II. Nonlinear Flight Dynamic Modeling

The proposed modeling methodology begins with the postulation of a nonlinear flight dynamic model for the aircraft of interest. Often, we consider an aircraft to be modeled as a rigid body of mass m. Let unit vectors $\{\boldsymbol{i}_1, \boldsymbol{i}_2, \boldsymbol{i}_3\}$ define an earth-fixed North-East-Down (NED) orthonormal reference frame, $\mathcal{F}_\mathrm{I}$. We assume $\mathcal{F}_\mathrm{I}$ well approximates an inertial reference frame over the time scales of interest. Let the unit vectors $\{\boldsymbol{b}_1, \boldsymbol{b}_2, \boldsymbol{b}_3\}$ define the orthonormal body-fixed frame, $\mathcal{F}_\mathrm{B}$, centered at the aircraft center of gravity (CG) with $\boldsymbol{b}_1$ out the front of the aircraft, $\boldsymbol{b}_2$ out of the right-hand side, and $\boldsymbol{b}_3$ out of the bottom. The moment of inertia matrix about the center of mass in $\mathcal{F}_\mathrm{B}$ is denoted $\boldsymbol{I}$. The position of the body frame with respect to the inertial frame is given by the vector $\boldsymbol{q} = [x\,y\,z]^\mathsf{T}$. The attitude of the aircraft is given by the rotation matrix $\boldsymbol{R}_\mathrm{IB}$ that maps free vectors from $\mathcal{F}_\mathrm{B}$ to $\mathcal{F}_\mathrm{I}$. Let $\boldsymbol{v} = [u\,v\,w]^\mathsf{T}$ and $\boldsymbol{\omega} = [p\,q\,r]^\mathsf{T}$ be the translational and rotational velocity of the aircraft with respect to $\mathcal{F}_\mathrm{I}$ and expressed in $\mathcal{F}_\mathrm{B}$, respectively. Thus, we have the kinematic equations of motion

$$\dot{\boldsymbol{q}} = \boldsymbol{R}_\mathrm{IB}\boldsymbol{v} \tag{1a}$$

$$\dot{\boldsymbol{R}}_\mathrm{IB} = \boldsymbol{R}_\mathrm{IB}[\boldsymbol{\omega}\times] \tag{1b}$$

where $[(\cdot)\times]$ is the skew-symmetric cross product equivalent matrix satisfying $[\boldsymbol{a}\times]\boldsymbol{b} = \boldsymbol{a} \times \boldsymbol{b}$ for 3-vectors $\boldsymbol{a}$ and $\boldsymbol{b}$. Consider the following Euler angle parameterization for $\boldsymbol{R}_\mathrm{IB}$:

$$\boldsymbol{R}_\mathrm{IB} = e^{[\boldsymbol{e}_3\times]\psi}e^{[\boldsymbol{e}_2\times]\theta}e^{[\boldsymbol{e}_1\times]\phi}$$

where ϕ, θ, and ψ are the roll, pitch, and yaw angles of the aircraft, respectively, and where $\boldsymbol{e}_1 = [1\,0\,0]^\mathsf{T}$, etc. With $\boldsymbol{\Theta} = [\phi\,\theta\,\psi]^\mathsf{T}$, Eq. (1b) becomes

$$\dot{\boldsymbol{\Theta}} = \underbrace{\begin{bmatrix} 1 & \sin\phi\tan\theta & \cos\phi\tan\theta \\ 0 & \cos\phi & -\sin\phi \\ 0 & \sin\phi\sec\theta & \cos\phi\sec\theta \end{bmatrix}}_{\boldsymbol{L}_\mathrm{IB}} \begin{bmatrix} p \\ q \\ r \end{bmatrix} \tag{2}$$

We represent the applied force and moment vectors expressed in $\mathcal{F}_\mathrm{B}$ as $\boldsymbol{F} = [F_x\,F_y\,F_z]^\mathsf{T}$ and $\boldsymbol{M} = [M_z\,M_y\,M_z]^\mathsf{T}$, respectively, where the specific dependence on body velocity, $\boldsymbol{v}$, angular velocity, $\boldsymbol{\omega}$, and an *actuator state vector*, $\boldsymbol{\Omega}$, is

left implicit for now. For example, these actuators may be control surface deflections of a fixed-wing aircraft or rotor speeds of a multirotor aircraft. We also parameterize the force and moment model by the vector of unknown parameters, $\boldsymbol{\vartheta}$, which we ultimately want to identify from large-domain flight data. Altogether, we have the nonlinear rigid body equations of motion

$$\dot{\boldsymbol{q}} = \boldsymbol{R}_{\mathrm{IB}}\boldsymbol{v} \tag{3a}$$

$$\dot{\boldsymbol{\Theta}} = \boldsymbol{L}_{\mathrm{IB}}\boldsymbol{\omega} \tag{3b}$$

$$\dot{\boldsymbol{v}} = \boldsymbol{v} \times \boldsymbol{\omega} + g\boldsymbol{R}_{\mathrm{IB}}^{\mathsf{T}}\boldsymbol{e}_3 + \frac{1}{m}\boldsymbol{F}(\boldsymbol{v},\boldsymbol{\omega},\boldsymbol{\Omega};\boldsymbol{\vartheta}) \tag{3c}$$

$$\dot{\boldsymbol{\omega}} = \boldsymbol{I}^{-1}\left(\boldsymbol{I}\boldsymbol{\omega} \times \boldsymbol{\omega} + \boldsymbol{M}(\boldsymbol{v},\boldsymbol{\omega},\boldsymbol{\Omega};\boldsymbol{\vartheta})\right) \tag{3d}$$

Eq. (3) can be written more compactly in terms of the system's *configuration*, $\boldsymbol{\xi} = [\boldsymbol{q}^{\mathsf{T}}\ \boldsymbol{\Theta}^{\mathsf{T}}]^{\mathsf{T}} \in \mathbb{R}^6$, and *generalized velocity*, $\boldsymbol{\nu} = [\boldsymbol{v}^{\mathsf{T}}\ \boldsymbol{\omega}^{\mathsf{T}}]^{\mathsf{T}} \in \mathbb{R}^6$. Let $\boldsymbol{f}_{\mathrm{a}} = [\boldsymbol{F}^{\mathsf{T}}\ \boldsymbol{M}^{\mathsf{T}}]^{\mathsf{T}}$ be the *generalized force* applied to the system. Then, we can write Eq. (3) as

$$\dot{\boldsymbol{\xi}} = \boldsymbol{f}_{\xi}(\boldsymbol{\xi},\boldsymbol{\nu}) \tag{4a}$$

$$\dot{\boldsymbol{\nu}} = \boldsymbol{f}_{\nu}(\boldsymbol{\xi},\boldsymbol{\nu}) + \mathscr{M}^{-1}\boldsymbol{f}_{\mathrm{a}}(\boldsymbol{\nu},\boldsymbol{\Omega};\boldsymbol{\vartheta}) \tag{4b}$$

where $\mathscr{M} = \mathbf{diag}(m\mathbb{I}, \boldsymbol{I})$ is the *generalized mass matrix* of the system. We call $\boldsymbol{f} = [\boldsymbol{f}_{\xi}^{\mathsf{T}}\ \boldsymbol{f}_{\nu}^{\mathsf{T}}]^{\mathsf{T}}$ the *acceleration vector field*, which contains the *known* dynamics of the system (kinematics, rotating reference frame effects, and gravity). The *aerodynamic model*, $\boldsymbol{f}_{\mathrm{a}}$, captures the hypothesized model structure which is parameterized by the unknown vector $\boldsymbol{\vartheta}$. It can be written as

$$\boldsymbol{f}_{\mathrm{a}}(\boldsymbol{\nu},\boldsymbol{\Omega};\boldsymbol{\vartheta}) = \boldsymbol{F}_{\mathrm{a}}(\boldsymbol{\Omega};\boldsymbol{\vartheta})\boldsymbol{\nu} + \boldsymbol{\varphi}(\boldsymbol{\nu}_{\mathrm{nl}},\boldsymbol{\Omega};\boldsymbol{\vartheta}) \tag{5}$$

where $\boldsymbol{F}_{\mathrm{a}}(\boldsymbol{\Omega};\boldsymbol{\vartheta}) \in \mathbb{R}^{6\times6}$ captures the aerodynamic effects that are linear in the generalized velocity and where $\boldsymbol{\nu}_{\mathrm{nl}}$ contains functions of the velocity variables that describe the model's *dominant nonlinearities*, $\boldsymbol{\varphi}$. Note that one could simply take $\boldsymbol{\nu}_{\mathrm{nl}} = \boldsymbol{\nu}$, but the reference signal and control design may be simpler for a different choice of $\boldsymbol{\nu}_{\mathrm{nl}}$. As an example, the longitudinal aerodynamics of a fixed-wing aircraft depend on the angle-of-attack, $\alpha = \tan^{-1}(w/u)$, which appears among the dominant nonlinearities (e.g., α and α^2 are important regressor functions).

As the example in this paper, we aim to obtain large-domain excitation data for the small quadrotor UAS shown in Figure 1. This aircraft was built using a DJI FlameWheel 450 frame and instrumented with a Cubepilot CubeOrange
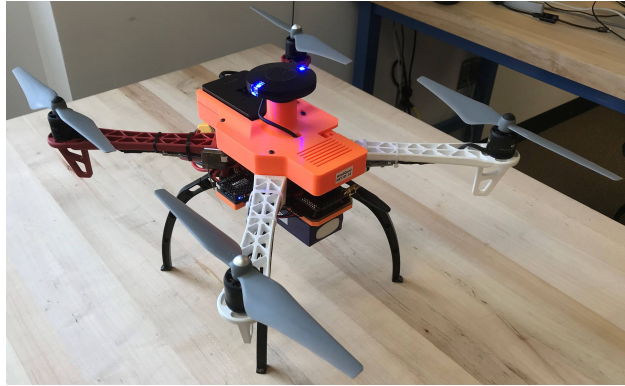

Fig. 1   Small quadrotor UAS.

flight computer running PX4 firmware. An onboard Raspberry Pi co-computer is included for control law and excitation implementation over MAVROS. The quadrotor was instrumented with CAN electronic speed controllers (ESCs) capable of rotor speed measurements and a real-time kinematics (RTK) capable GNSS receiver. The instrumentation, co-computer setup, and data processing for this aircraft followed the methods detailed in [9, 10].

The quadrotor aircraft considered here is a symmetric "X" configuration as pictured in Figure 2, where Ω_i is the angular speed of the ith rotor, ℓ is the rotor arm length, h is the height of the rotor hubs above the center of gravity, and $\sigma_i \in \{+1, -1\}$ is the direction of the ith rotor according to the right-hand rule in the body frame. The applied
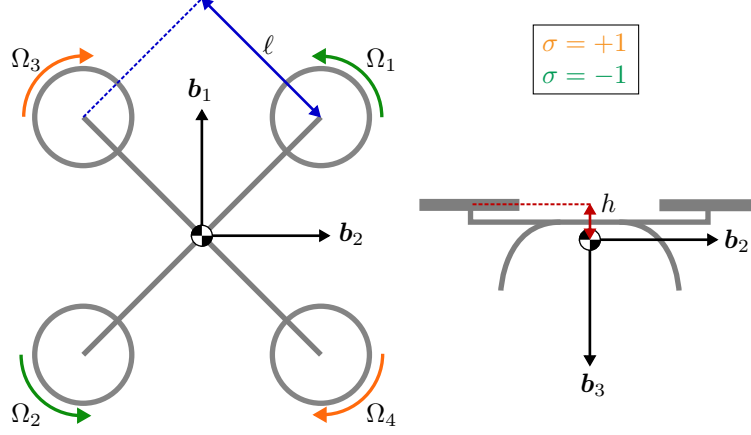
Fig. 2   Quadrotor geometry

force and moment on the rigid body can be derived using blade-element and momentum theory as detailed in [11]. Considering a second-order Taylor series expansion (Model 3 in [11]), the components of the applied force and moment vectors can be modeled as

$$F_x = K_{x_{\mu_0}} u + K_{x_{\mu_w}} uw + K_{x_{\mu_b}} u\delta t \tag{6a}$$

$$F_y = K_{y_{\mu_0}} v + K_{y_{\mu_w}} vw + K_{y_{\mu_b}} v\delta t \tag{6b}$$

$$F_z = K_{z_{T_0}} \delta^2 t + K_{z_{\mu_0}} \delta t + K_{z_\mu} (u^2 + v^2) + K_{z_{\mu_w}} (4w\delta t - p\delta a - q\delta e) \tag{6c}$$

$$M_x = K_{l_{T_0}} \delta^2 a + K_{l_{\mu_0}} \delta a + K_{l_{\mu_w}} (w\delta a - 2\ell^2 p\delta t - \ell^2 q\delta r/2) + K_{l_{\mu_b}} v\delta t$$
$$\qquad + K_{l_{\mu_b,\mu_0}} v + K_{l_{\mu_b,\mu_w}} vw + K_{l_{\delta_r}} u\delta r \tag{6d}$$

$$M_y = K_{m_{T_0}} \delta^2 e + K_{m_{\mu_0}} \delta e + K_{m_{\mu_w}} (w\delta e - 2\ell^2 q\delta t - \ell^2 p\delta r/2) + K_{m_{\mu_b}} u\delta t$$
$$\qquad + K_{m_{\mu_b,\mu_0}} u + K_{m_{\mu_b,\mu_w}} uw + K_{m_{\delta_r}} v\delta r \tag{6e}$$

$$M_z = K_{n_{Q_0}} \delta^2 r + K_{n_{\mu_0}} \delta r + K_{n_{\mu_w}} (w\delta r + p\delta e + q\delta a) + K_{n_{\mu_w^2}} pq$$
$$\qquad + K_{n_{\mu_b}} (u\delta a + v\delta e) + K_{n_{\mu_b,\mu_w}} (up + vq) + J_z p\dot{\delta r} \tag{6f}$$

where $K_{(\cdot)}$ are lumped parameters with appropriate dimensions, J_z is the motor moment of inertia, and the virtual actuators $\boldsymbol{\delta} = [\delta_t \ \delta_a \ \delta_e \ \delta_r]^\mathsf{T}$ and $\boldsymbol{\delta}^2 = [\delta_t^2 \ \delta_a^2 \ \delta_e^2 \ \delta_r^2]^\mathsf{T}$ are given by

$$\underbrace{\begin{bmatrix} \delta_t \\ \delta_a \\ \delta_e \\ \delta_r \end{bmatrix}}_{\boldsymbol{\delta}} := \underbrace{\begin{bmatrix} 1/4 & 1/4 & 1/4 & 1/4 \\ -\ell\sqrt{2}/2 & \ell\sqrt{2}/2 & \ell\sqrt{2}/2 & -\ell\sqrt{2}/2 \\ \ell\sqrt{2}/2 & -\ell\sqrt{2}/2 & \ell\sqrt{2}/2 & -\ell\sqrt{2}/2 \\ 1 & 1 & -1 & -1 \end{bmatrix}}_{\mathbf{M_{ix}}} \underbrace{\begin{bmatrix} \Omega_1 \\ \Omega_2 \\ \Omega_3 \\ \Omega_4 \end{bmatrix}}_{\boldsymbol{\Omega}^2} \quad \text{and} \quad \underbrace{\begin{bmatrix} \delta_t^2 \\ \delta_a^2 \\ \delta_e^2 \\ \delta_r^2 \end{bmatrix}}_{\boldsymbol{\delta}^2} := \mathbf{M_{ix}} \underbrace{\begin{bmatrix} \Omega_1^2 \\ \Omega_2^2 \\ \Omega_3^2 \\ \Omega_4^2 \end{bmatrix}}_{\boldsymbol{\Omega}^2} \tag{7}$$

The uncertain parameters which we ultimately want to identify for the nonlinear model are $\boldsymbol{\vartheta} = [K_{(\cdot)}]$.

Since the virtual actuators are neither independently nor directly controlled, we adopt the first-order motor model

$$\dot{\boldsymbol{\Omega}} = -a_\Omega \boldsymbol{\Omega} + b_\Omega \boldsymbol{u}_{\text{ESC}} \tag{8}$$

where a_Ω and b_Ω are uncertain parameters and $\boldsymbol{u}_{\text{ESC}}$ is a command vector sent to the motor electronic speed controllers. The choice of this uncertainty allows for the true values of a_Ω and b_Ω to change over the course of the flight as they generally depend on battery voltage [12]. Because of interdependence between the virtual actuators, we consider the rotor speed vector, $\boldsymbol{\Omega}$, to be the actuator state vector, $\boldsymbol{\Omega}$, in Eq. (4). To retain the physical meaning of the virtual actuators defined above, we choose the control input to the system to be the *virtual actuator command*, $\boldsymbol{u} = [u_t \ u_a \ u_e \ u_r]^\mathsf{T} = \mathbf{M_{ix}} \boldsymbol{u}_{\text{ESC}}$.

Comparing Eq. (6) with Eq. (5), we see the state variables that capture the model's nonlinearities are the components of $\boldsymbol{\nu}_{\mathrm{nl}} = \boldsymbol{v}$. Therefore, we choose to design a reference signal that effectively covers the desired domain of body velocity along with a robust control law that keeps correlation among regressors low while also guaranteeing stability.

III. Linear Parameter-Varying Model

With the system's dominant nonlinearities specified, the next step is to formulate the system dynamics as an LPV system with $\boldsymbol{\nu}_{\mathrm{nl}}$ as the scheduling "quasi-parameter" (recognizing that $\boldsymbol{\nu}_{\mathrm{nl}}$ is, in fact, part of the system state). This allows a control law to be readily designed that stabilizes some desired reference signal for $\boldsymbol{\nu}_{\mathrm{nl}}$.

Since the dominant nonlinearities of the quadrotor model depend on body velocity, $\boldsymbol{v}$, we desire $\boldsymbol{v}$ to track some *a priori* reference signal $\boldsymbol{v}_{\mathrm{d}}(t)$ – the scheduling quasi-parameter for the LPV system. For each fixed $\boldsymbol{v}_{\mathrm{d}}$, we linearize the system about the equilibrium condition defined by $\boldsymbol{\Theta} = \boldsymbol{\Theta}_0$, $\boldsymbol{v} = \boldsymbol{v}_{\mathrm{d}}$, $\boldsymbol{\omega} = \boldsymbol{0}$, and $\boldsymbol{\Omega} = \boldsymbol{\Omega}_0$. To simplify the LPV system formulation, we make the following assumption.

Assumption 1 *The steady-state roll angle, pitch angle, and motor speeds in translating flight, depend linearly on body velocity:*

$$\begin{bmatrix} \phi_0(\boldsymbol{v}_{\mathrm{d}}) \\ \theta_0(\boldsymbol{v}_{\mathrm{d}}) \\ \boldsymbol{\Omega}_0(\boldsymbol{v}_{\mathrm{d}}) \end{bmatrix} = \boldsymbol{\Lambda}\boldsymbol{v}_{\mathrm{d}} + \begin{bmatrix} 0 \\ 0 \\ \boldsymbol{\Omega}_{\mathrm{hover}} \end{bmatrix} \tag{9a}$$

where $\boldsymbol{\Lambda}$ is some constant matrix and $\boldsymbol{\Omega}_{\mathrm{hover}}$ is the vector of motor speeds in hover.

Next, we compute the Jacobians of the aerodynamic model,

$$\mathcal{A} = \left.\frac{\partial \boldsymbol{f}_a}{\partial \boldsymbol{\nu}}\right|_{(\boldsymbol{v}_{\mathrm{d}},\boldsymbol{0},\boldsymbol{\Omega}_0(\boldsymbol{v}_{\mathrm{d}}))} \qquad \text{and} \qquad \mathcal{B}_{\Omega} = \left.\frac{\partial \boldsymbol{f}_a}{\partial \boldsymbol{\Omega}}\right|_{(\boldsymbol{v}_{\mathrm{d}},\boldsymbol{0},\boldsymbol{\Omega}_0(\boldsymbol{v}_{\mathrm{d}}))} \tag{10}$$

Since the chosen control input, $\boldsymbol{u}$, is the commanded virtual actuator vector (as opposed to motor commands), let

$$\mathcal{B} = \mathcal{B}_{\Omega}\mathrm{M}_{\mathrm{ix}}^{-1} \tag{11}$$

The matrices $\mathcal{A}$ and $\mathcal{B}$ have affine dependence on $\boldsymbol{v}_{\mathrm{d}}$:

$$\mathcal{A} = \mathcal{A}_0 + \mathcal{A}_u u_{\mathrm{d}} + \mathcal{A}_v v_{\mathrm{d}} + \mathcal{A}_w w_{\mathrm{d}} \tag{12a}$$
$$\mathcal{B} = \mathcal{B}_0 + \mathcal{B}_u u_{\mathrm{d}} + \mathcal{B}_v v_{\mathrm{d}} + \mathcal{B}_w w_{\mathrm{d}} \tag{12b}$$

where the elements of the matrices $\mathcal{A}_{(\cdot)}$ and $\mathcal{B}_{(\cdot)}$ that are functions of the unknown parameter vector, $\boldsymbol{\vartheta}$, are given in Appendix A.

For the LPV model of the aircraft dynamics, consider the following simplifying assumption.

Assumption 2 *The roll and pitch angles remain sufficiently small such that the acceleration vector field in Eq. (4) can be taken to be linear in $\boldsymbol{\xi}$ and $\boldsymbol{\nu}$, with affine dependence on the scheduling parameter $\boldsymbol{v}_{\mathrm{d}}$. That is,*

$$\boldsymbol{f}(\boldsymbol{\xi},\boldsymbol{\nu}) = \boldsymbol{f}(\boldsymbol{\xi}_0(\boldsymbol{v}_{\mathrm{d}}),\boldsymbol{\nu}_0(\boldsymbol{v}_{\mathrm{d}})) + \boldsymbol{A}_{\xi}(\boldsymbol{v}_{\mathrm{d}})(\boldsymbol{\xi} - \boldsymbol{\xi}_0(\boldsymbol{v}_{\mathrm{d}})) + \boldsymbol{A}_{\nu}(\boldsymbol{v}_{\mathrm{d}})(\boldsymbol{\nu} - \boldsymbol{\nu}_0(\boldsymbol{v}_{\mathrm{d}})) \tag{13}$$

where $\boldsymbol{A}_{\xi}(\boldsymbol{v}_{\mathrm{d}}) = \left.\frac{\partial \boldsymbol{f}}{\partial \boldsymbol{\xi}}\right|_{(\boldsymbol{\xi}_0(\boldsymbol{v}_{\mathrm{d}}),\boldsymbol{\nu}_0(\boldsymbol{v}_{\mathrm{d}}))}$ and $\boldsymbol{A}_{\nu}(\boldsymbol{v}_{\mathrm{d}}) = \left.\frac{\partial \boldsymbol{f}}{\partial \boldsymbol{\nu}}\right|_{(\boldsymbol{\xi}_0(\boldsymbol{v}_{\mathrm{d}}),\boldsymbol{\nu}_0(\boldsymbol{v}_{\mathrm{d}}))}$ are affine in $\boldsymbol{v}_{\mathrm{d}}$.

Assumption 2 effectively defines an implicit relationship between roll/pitch angles and body velocity such that the nonlinearities in $\boldsymbol{R}_{\mathrm{IB}}$ and $\boldsymbol{L}_{\mathrm{IB}}$ are replaced by linear dependence on $\boldsymbol{\Theta}$ which in turn depends linearly on $\boldsymbol{v}_{\mathrm{d}}$. Let

$$\Delta\boldsymbol{x} = \begin{bmatrix} \Delta\boldsymbol{\xi} \\ \Delta\boldsymbol{\nu} \\ \Delta\boldsymbol{\delta} \end{bmatrix} \tag{14}$$

where $\Delta\boldsymbol{\xi} = \boldsymbol{\xi} - \boldsymbol{\xi}_0(\boldsymbol{v}_{\mathrm{d}})$, $\Delta\boldsymbol{\nu} = \boldsymbol{\nu} - \boldsymbol{\nu}_0(\boldsymbol{v}_{\mathrm{d}})$, and $\Delta\boldsymbol{\delta} = \mathbf{M_{ix}}\Delta\boldsymbol{\Omega} = \boldsymbol{\Omega} - \boldsymbol{\Omega}_0(\boldsymbol{v}_{\mathrm{d}})$. Also, let $\Delta\boldsymbol{u} = \boldsymbol{u} - \boldsymbol{u}_0(\boldsymbol{v}_{\mathrm{d}})$ be the input perturbation. Then, an LPV model of the system can be written as

$$
\begin{bmatrix} \Delta\dot{\boldsymbol{\xi}} \\ \Delta\dot{\boldsymbol{\nu}} \\ \Delta\dot{\boldsymbol{\delta}} \end{bmatrix} = \left(\underbrace{\begin{bmatrix} \boldsymbol{A}_\xi(\boldsymbol{v}_{\mathrm{d}}) & \boldsymbol{A}_\nu(\boldsymbol{v}_{\mathrm{d}}) & \boldsymbol{0} \\ \boldsymbol{0} & \boldsymbol{0} & \boldsymbol{0} \end{bmatrix} + \begin{bmatrix} \boldsymbol{0} & \boldsymbol{0} & \boldsymbol{0} \\ \boldsymbol{0} & \mathscr{M}^{-1}\boldsymbol{\mathcal{A}}(\boldsymbol{v}_{\mathrm{d}}) & \mathscr{M}^{-1}\boldsymbol{\mathcal{B}}(\boldsymbol{v}_{\mathrm{d}}) \\ \boldsymbol{0} & \boldsymbol{0} & -a_\Omega\mathbb{I} \end{bmatrix}}_{\boldsymbol{A}} \right) \begin{bmatrix} \Delta\boldsymbol{\xi} \\ \Delta\boldsymbol{\nu} \\ \Delta\boldsymbol{\delta} \end{bmatrix} + \underbrace{\begin{bmatrix} \boldsymbol{0} \\ \boldsymbol{0} \\ b_\Omega\mathbb{I} \end{bmatrix}}_{\boldsymbol{B}} \Delta\boldsymbol{u} \quad (15)
$$

More compactly, we have

$$
\Delta\dot{\boldsymbol{x}} = \boldsymbol{A}(\boldsymbol{v}_{\mathrm{d}}, \boldsymbol{\theta})\Delta\boldsymbol{x} + \boldsymbol{B}(\boldsymbol{\theta})\Delta\boldsymbol{u} \tag{16}
$$

where $\boldsymbol{\theta}$ is the vector of unknown elements of the constant matrices that define the affine LPV system in Eq. (15).

Since we are simultaneously stabilizing a reference trajectory and exciting the aircraft dynamics about it, we decompose the input vector, $\boldsymbol{u}$, into two parts – a control input $\boldsymbol{u}_{\mathrm{c}}$ and a normalized excitation input $\boldsymbol{u}_{\mathrm{e}}$. In general, we write

$$
\boldsymbol{u} = \boldsymbol{u}_{\mathrm{c}} + \boldsymbol{R}\boldsymbol{u}_{\mathrm{e}} \tag{17}
$$

for some constant invertible scaling matrix $\boldsymbol{R}$ that defines the effective excitation input $\tilde{\boldsymbol{u}}_{\mathrm{e}} = \boldsymbol{R}\boldsymbol{u}_{\mathrm{e}}$. We also define a performance output that represents some scaled value of the perturbation from the desired velocity reference:

$$
\boldsymbol{z} = \boldsymbol{Q}^{-1}(\boldsymbol{v} - \boldsymbol{v}_{\mathrm{d}}) = \boldsymbol{Q}^{-1}\Delta\boldsymbol{v} \tag{18}
$$

for some constant invertible matrix $\boldsymbol{Q}$. Thus, the LPV system (16) is now written as

$$
\Delta\dot{\boldsymbol{x}} = \boldsymbol{A}(\boldsymbol{v}_{\mathrm{d}}, \boldsymbol{\theta})\Delta\boldsymbol{x} + \boldsymbol{B}_{\mathrm{c}}(\boldsymbol{\theta})\Delta\boldsymbol{u}_{\mathrm{c}} + \boldsymbol{B}_{\mathrm{e}}(\boldsymbol{\theta})\boldsymbol{u}_{\mathrm{e}} \tag{19a}
$$
$$
\boldsymbol{z} = \boldsymbol{C}\Delta\boldsymbol{x} \tag{19b}
$$

where $\boldsymbol{B}_{\mathrm{c}} = \boldsymbol{B}$, $\boldsymbol{B}_{\mathrm{e}} = \boldsymbol{B}\boldsymbol{R}$, and the output matrix $\boldsymbol{C}$ is constructed using Eq. (18).

Since every affine description can be written as a polytopic one (see [13] and the references therein), we represent the LPV system in Eq. (19) as polytopic in the scheduling variable, $\boldsymbol{v}_{\mathrm{d}}$. Let

$$
\boldsymbol{v}_{\mathrm{d}} \in [\boldsymbol{v}_{\min}, \boldsymbol{v}_{\max}] =: \mathbb{P}_{v_{\mathrm{d}}} \tag{20}
$$

Then we can write the system in Eq. (19) as the convex combination

$$
\boldsymbol{\Lambda}(\boldsymbol{v}_{\mathrm{d}}, \boldsymbol{\theta}) := \begin{bmatrix} \boldsymbol{A}(\boldsymbol{v}_{\mathrm{d}}, \boldsymbol{\theta}) & \boldsymbol{B}_{\mathrm{c}}(\boldsymbol{\theta}) & \boldsymbol{B}_{\mathrm{e}}(\boldsymbol{\theta}) \\ \boldsymbol{C} & \boldsymbol{0} & \boldsymbol{0} \end{bmatrix} = \sum_{i=1}^{N} \alpha_i(\boldsymbol{v}_{\mathrm{d}}) \begin{bmatrix} \boldsymbol{A}_i(\boldsymbol{\theta}) & \boldsymbol{B}_{\mathrm{c}}(\boldsymbol{\theta}) & \boldsymbol{B}_{\mathrm{e}}(\boldsymbol{\theta}) \\ \boldsymbol{C} & \boldsymbol{0} & \boldsymbol{0} \end{bmatrix} =: \sum_{i=1}^{N} \alpha_i(\boldsymbol{v}_{\mathrm{d}})\boldsymbol{\Lambda}_i(\boldsymbol{\theta}) \quad (21)
$$

where

$$
\sum_{i=1}^{N} \alpha_i(\boldsymbol{v}_{\mathrm{d}}) = 1
$$

This equation defines a polytope with $N = 2^3$ vertices given by the corners of the box constraint in Eq. (20), where each vertex system, $\boldsymbol{\Lambda}_i(\boldsymbol{\theta})$ is uncertain for

$$
\boldsymbol{\theta} \in [\boldsymbol{\theta}_{\min}, \boldsymbol{\theta}_{\max}] =: \mathbb{P}_\theta \tag{22}
$$

Thus for each $i \in \{1, \ldots, N\}$, we have

$$
\boldsymbol{\Lambda}_i(\boldsymbol{\theta}) = \sum_{j=1}^{M_i} \beta_i^j(\boldsymbol{\theta}) \begin{bmatrix} \boldsymbol{A}_i^j & \boldsymbol{B}_{\mathrm{c}}^j & \boldsymbol{B}_{\mathrm{e}}^j \\ \boldsymbol{C} & \boldsymbol{0} & \boldsymbol{0} \end{bmatrix} =: \sum_{j=1}^{M_i} \beta_i^j(\boldsymbol{\theta})\boldsymbol{\Lambda}_i^j, \quad \sum_{j=1}^{M_i} \beta_i^j(\boldsymbol{\theta}) = 1 \tag{23}
$$

Therefore, in order to design a control law we need only identify small perturbation linear models for each ith vertex of the polytopic LPV system. The uncertainty polytope vertices are then defined using the parameter confidence intervals found in the parameter estimation process. The resulting description of the system is a nested polytope, as depicted in Figure 3 for two scheduling parameters ρ_1 and ρ_2. In this figure, each point in the scheduling parameter space contained within the blue polytope defines an uncertain LTI system. The true LTI system at that parameter value is defined at some point in the orange polytope, which lies in the uncertain parameter space (axes not shown).
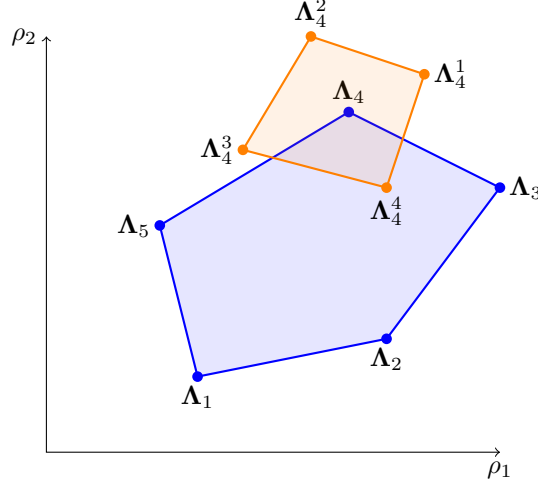
Fig. 3   Nested polytopic description.

IV. Vertex Model Identification

In order to proceed with identification of the polytopic LPV model (21), we assume there exists a set of baseline control laws that locally stabilize the set of steady flight conditions defined by the vertices of the polytope, $\mathbb{P}_{v_\mathrm{d}}$. This is often a model-free control law such as proportional-integral-derivative (PID) control. Using this control law, flight test data is collected at the vertices of $\mathbb{P}_{v_\mathrm{d}}$. In this initial model identification process, the parametric uncertainty is also accurately characterized, yielding the polytopic uncertain LPV model (23).

For each LPV vertex system, we identify the elements of each matrix $\boldsymbol{A}_i$ that depend on unknown aerodynamic parameters, $K_{(.)}$, from flight data. The parameters a_Ω and b_Ω, however, are identified separately from flight data. For the specific aircraft considered in this work, they were found to be $a_\Omega = 12.31 \pm 0.21$ and $b_\Omega = (1.399 \pm 0.182) \times 10^4$. Each of the vertex LTI models was identified using the equation-error "grey-box" identification process detailed in Appendix B. This method solves the parameter estimation problem using ordinary least-squares for the unknown elements of each $\boldsymbol{A}_i$.

Due to hardware implementation restrictions, the quadrotor LTI dynamics were excited using body velocity and yaw rate reference commands. This was mainly due to the inability to command "broken-loop" excitation signals from the co-computer over MAVROS. Although the use of velocity commands is not ideal because the resulting actuator states may be correlated, this choice of excitation makes initial model identification easier and was found to be sufficient for the initial phase of model identification. The reference command excitation signal was a 4-axis, 30 second multisine signal with uniform power spectral density in the frequency range from 0.2 to 2 Hz, generated using SIDPAC software [14]. The multisine body velocity reference components were superimposed over constant body velocity commands corresponding to the vertices of the LPV polytope described in Section III.

For this example, the maximum and minimum velocities were chosen to be $+5$ m/s and -5 m/s, respectively, in all components. For the flight test data collection, the constant body velocity reference was commanded for 10 seconds prior to excitation to allow for experimental determination of the equilibrium flight condition, $\{\boldsymbol{x}_0(\boldsymbol{v}_\mathrm{d}), \boldsymbol{u}_0(\boldsymbol{v}_\mathrm{d})\}$. Because the baseline controller performance is limited, the equilibrium condition from flight data does not perfectly align with the commanded velocity, as shown in Table 1. Note, in particular, that for vertices corresponding to descending flight, the magnitude of the actual downward velocity (w_0) is much smaller than the commanded value. The equation error least squares parameter estimation was conducted for each axis of each vertex system using these data. The results are tabulated in Table 2. The coefficient of determination is poor for flight conditions where the quadrotor is descending through its rotor wake. We note, however, that poor results are perfectly acceptable for the proposed use, provided the parametric *uncertainty* is well characterized for the robust LPV controller.

The identified LTI models along with the estimated parameter variances were used to define the uncertain LPV model described by Eq. (19). This model was then validated against an independent maneuver generated with a 4-axis multisine about the hover condition. From this maneuver, the time derivative of the state vector from flight data, $\dot{\boldsymbol{x}}_\mathrm{f}$, was obtained along with the modeled state derivative from Eq. (19), $\dot{\boldsymbol{x}}_\mathrm{m}$. The validation time history of K samples is shown in Figure 4. Let $\dot{\boldsymbol{x}}_{\mathrm{m},i}$ and $\dot{\boldsymbol{x}}_{\mathrm{f},i}$ be the $K \times 1$ column vectors containing the time history of the respective time

Table 1   Flight Data Vertex Equilibria

Vertex	u_0	v_0	w_0	ϕ_0	θ_0	$\delta_{t,0}$	$\delta_{a,0}$	$\delta_{e,0}$	$\delta_{r,0}$
	[m/s]	[m/s]	[m/s]	[deg]	[deg]	[rad/s]	[rad/s]	[rad/s]	[rad/s]
$[-5 \;\; -5 \;\; -5]^\mathsf{T}$	-4.99	-5.04	-4.20	-10.87	9.28	691.4	-36.7	29.0	310.5
$[+5 \;\; -5 \;\; -5]^\mathsf{T}$	4.95	-5.04	-4.17	-10.44	-8.05	685.0	-34.1	-1.5	39.2
$[-5 \;\; +5 \;\; -5]^\mathsf{T}$	-5.01	5.03	-3.95	8.55	8.11	689.0	-2.8	25.3	34.9
$[+5 \;\; +5 \;\; -5]^\mathsf{T}$	5.03	5.01	-4.00	8.04	-8.98	679.5	-5.8	-4.0	305.4
$[-5 \;\; -5 \;\; +5]^\mathsf{T}$	-4.83	-4.68	2.88	-5.00	3.17	554.9	-45.0	28.0	367.6
$[+5 \;\; -5 \;\; +5]^\mathsf{T}$	4.73	-4.61	2.72	-5.14	-4.08	521.8	-34.6	-18.3	158.9
$[-5 \;\; +5 \;\; +5]^\mathsf{T}$	-4.85	4.75	3.00	3.80	3.00	546.9	14.0	23.4	-9.8
$[+5 \;\; +5 \;\; +5]^\mathsf{T}$	4.64	4.73	2.86	3.85	-4.83	525.8	3.49	-15.8	298.1

Table 2   LTI Equation Error Coefficient of Determination, R^2 [%]

			LTI State Equation Axis			
Nominal Vertex	$\dot{u}$	$\dot{v}$	$\dot{w}$	$\dot{p}$	$\dot{q}$	$\dot{r}$
$[-5 \;\; -5 \;\; -5]^\mathsf{T}$	30.1	39.3	81.2	83.2	88.9	95.5
$[+5 \;\; -5 \;\; -5]^\mathsf{T}$	39.8	29.9	86.4	84.0	91.4	94.1
$[-5 \;\; +5 \;\; -5]^\mathsf{T}$	40.4	38.1	78.8	76.8	84.5	95.4
$[+5 \;\; +5 \;\; -5]^\mathsf{T}$	38.6	33.2	69.7	80.0	85.0	94.6
$[-5 \;\; -5 \;\; +5]^\mathsf{T}$	9.4	15.7	97.8	80.2	75.2	95.0
$[+5 \;\; -5 \;\; +5]^\mathsf{T}$	19.8	12.6	98.9	75.4	85.1	96.6
$[-5 \;\; +5 \;\; +5]^\mathsf{T}$	10.7	18.3	96.5	80.3	85.3	93.7
$[+5 \;\; +5 \;\; +5]^\mathsf{T}$	17.4	14.3	97.6	79.0	83.3	95.9

derivatives for the ith state. Theil's inequality coefficient (TIC),

$$\mathrm{TIC} = \frac{\sqrt{\frac{1}{K}(\dot{\boldsymbol{x}}_{\mathrm{m},i} - \dot{\boldsymbol{x}}_{\mathrm{f},i})^\mathsf{T}(\dot{\boldsymbol{x}}_{\mathrm{m},i} - \dot{\boldsymbol{x}}_{\mathrm{f},i})}}{\sqrt{\frac{1}{K}\dot{\boldsymbol{x}}_{\mathrm{m},i}^\mathsf{T}\dot{\boldsymbol{x}}_{\mathrm{m},i}} + \sqrt{\frac{1}{K}\dot{\boldsymbol{x}}_{\mathrm{f},i}^\mathsf{T}\dot{\boldsymbol{x}}_{\mathrm{f},i}}} \tag{24}$$

and normalized root-mean squared error (NRMSE),

$$\mathrm{NRMSE} = \frac{1}{\mathrm{range}(\dot{\boldsymbol{x}}_{\mathrm{f},i})}\sqrt{\frac{1}{K}(\dot{\boldsymbol{x}}_{\mathrm{m},i} - \dot{\boldsymbol{x}}_{\mathrm{f},i})^\mathsf{T}(\dot{\boldsymbol{x}}_{\mathrm{m},i} - \dot{\boldsymbol{x}}_{\mathrm{f},i})} \tag{25}$$

were then computed and are given in Table 3. The model validates well with small values of TIC and NRMSE, especially in the translational dynamics. There is a slight bias apparent in the rotational dynamics, causing larger values of TIC and NRMSE.

Table 3   LPV model validation metrics

Axis	$\dot{u}$	$\dot{v}$	$\dot{w}$	$\dot{p}$	$\dot{q}$	$\dot{r}$
TIC	0.110	0.049	0.104	0.274	0.355	0.352
NRMSE	0.036	0.021	0.035	0.094	0.119	0.148
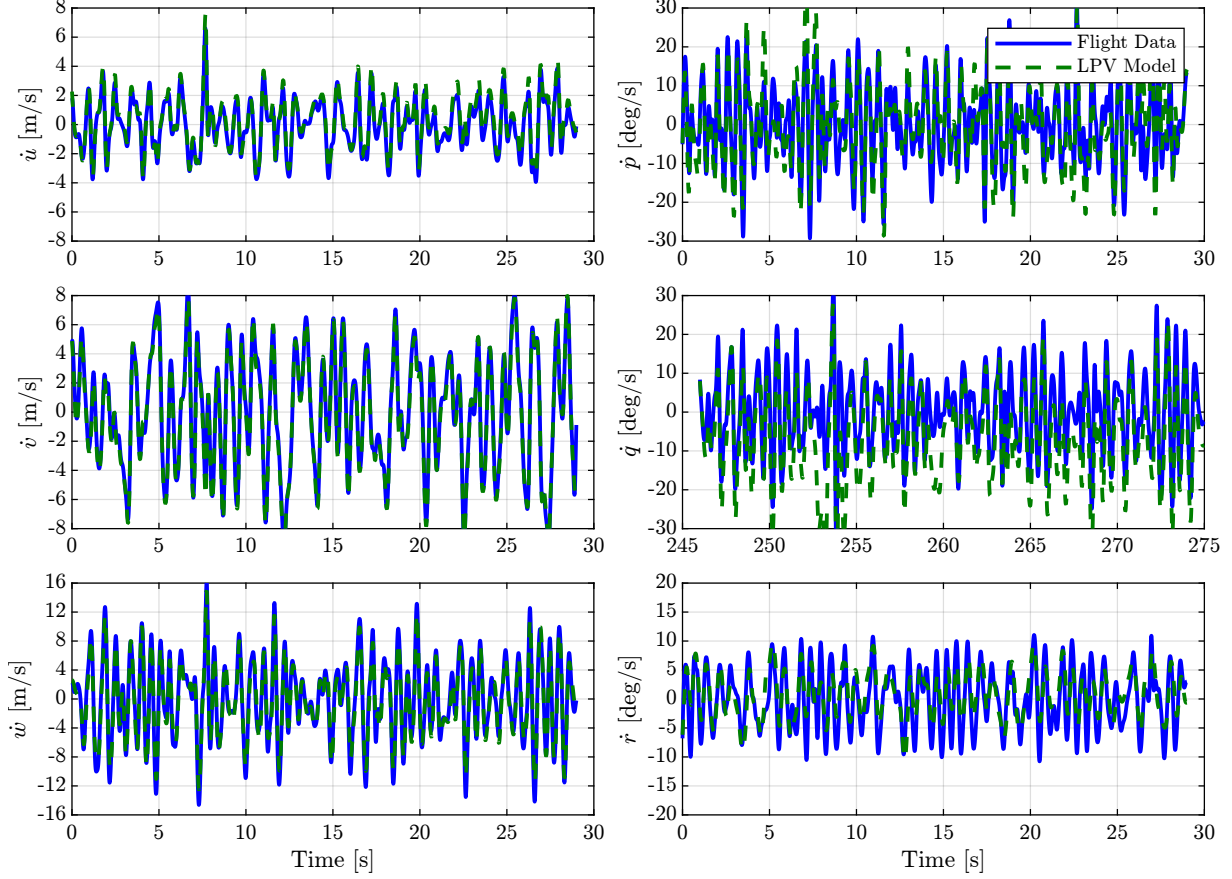
Fig. 4   LPV model independent validation.

V. Signal Design

With the polytopic LPV model identified and parametric uncertainty characterized, we can design the input signals to be used in the nonlinear model identification experiments. The two signals that need to be designed are the body velocity reference, $v_d(t)$, that covers the desired domain and the superposed command signal u_e that is intended to excite the vehicle dynamics about the reference motion. Since body velocity is an explanatory variable which appears in regressor functions that also depend nonlinearly on actuator states, δ, we want to ensure the v_d and u_e are uncorrelated. An efficient way to accomplish this is to design multisine signals for v_d and u_e concurrently such that they are orthogonal and phase-optimized [15]. Inspired by [16], we select the frequency range of the velocity reference to be sufficiently low in the interval $[0.01, 0.5]$ Hz, while the motor excitation signals are higher-frequency, in the interval $(0.5, 5]$ Hz. The upper limit on the excitation frequency was chosen based on recommendations from [17], but slightly lower due to concerns about damaging the ESCs. Another approach for determining the appropriate frequency range is to analyze the vehicle's response to frequency sweep data in each of the virtual actuators. Using SIDPAC's `mkmsswp.m` function, these signals were generated and are shown in Figure 5, normalized to unit amplitude, with their spectral content given in Figure 6. The correlation coefficients and plots of this signal are displayed in Figure 7, showing good coverage of the velocity space in the v_d signals and proper decorrelation overall.

Since the excitation input of T seconds is known, we can now make an informed choice of the performance output weighting, Q, and excitation input weighting, R. While in typical H_∞ control approaches the exogenous input is unknown, that is not the case here; we have direct knowledge of the "disturbance" that is perturbing the vehicle motion from equilibrium flight. We select tunable excitation input magnitudes Δ_t, Δ_a, Δ_e, and Δ_r. Then, the R matrix is chosen such that a normalized excitation input, u_e, that is defined to have unit energy,

$$\sqrt{\int_0^T u_e^\mathsf{T}(t) u_e(t) \mathrm{d}t} = 1 \tag{26}$$
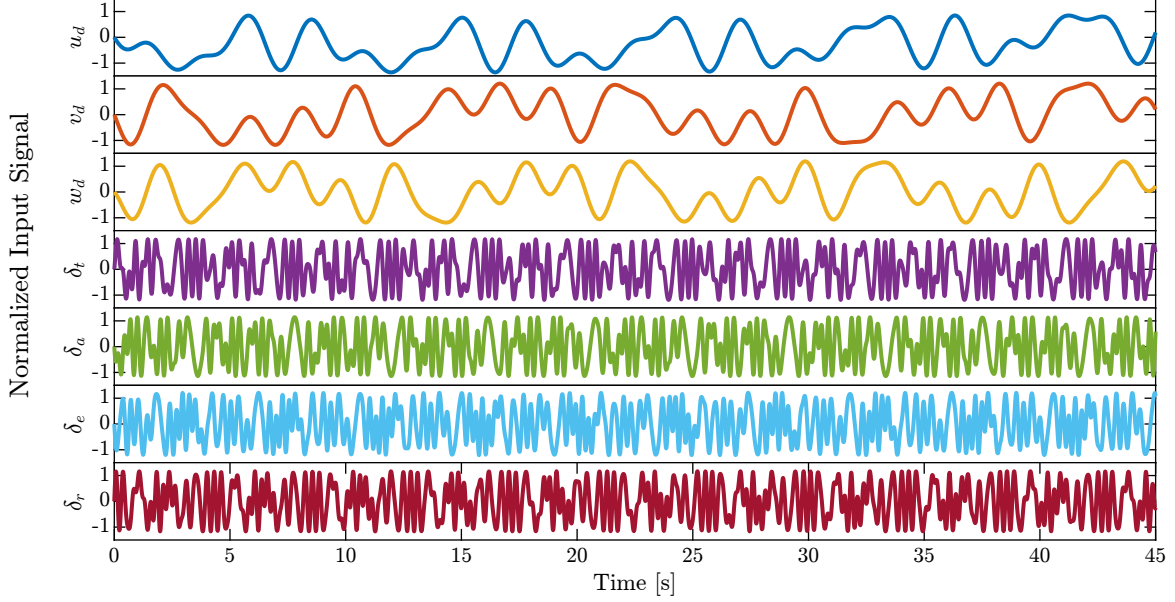
Fig. 5 Velocity reference and motor excitation multisine signal.
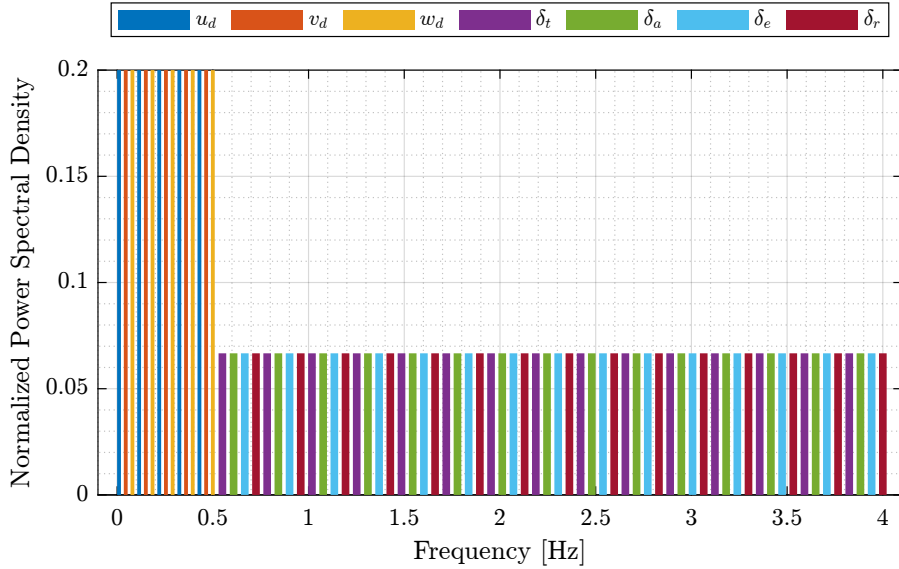
Fig. 6 Velocity reference and motor excitation multisine spectra.

results in the effective excitation inputs having magnitudes Δ_t, Δ_a, Δ_e, and Δ_r. Thus, $\boldsymbol{R}$ is defined as

$$\boldsymbol{R} = \sqrt{\frac{n_u T}{2}}\,\mathbf{diag}(\Delta_t, \Delta_a, \Delta_e, \Delta_r) \tag{27}$$

where $n_u = 4$. Similarly, we define maximum body velocity perturbations Δ_u, Δ_v, and Δ_w. The performance output, $\boldsymbol{z} = \boldsymbol{Q}^{-1}\Delta\boldsymbol{v}$, is then scaled such that the worst-case velocity perturbations corresponding to step changes of Δ_u, Δ_v, and Δ_w will generate a performance output that also has unit energy. Therefore, $\boldsymbol{Q}$ is chosen to be

$$\boldsymbol{Q} = \sqrt{n_z T}\,\mathbf{diag}(\Delta_u, \Delta_v, \Delta_w) \tag{28}$$

where $n_z = 3$. Note the factor of $1/\sqrt{2}$ that appears in $\boldsymbol{R}$ is not present in $\boldsymbol{Q}$ due to the asymmetry of the worst-case

10

Fig. 7   Velocity reference and motor excitation multisine correlation.

step perturbations mentioned above. This normalization provides a clear control objective of ensuring that the worst case energy gain from the normalized excitation input, $\boldsymbol{u}_{\mathrm{e}}$, to the normalized performance output, $\boldsymbol{z}$, is no greater than one.

Recall a signal $\boldsymbol{\xi}$ is said to be an element of the vector space L_2 if its L_2 norm is finite, meaning

$$\|\boldsymbol{\xi}\|_{L_2} = \sqrt{\int_0^\infty \boldsymbol{\xi}^{\mathsf{T}}(t)\boldsymbol{\xi}(t)\mathrm{d}t} < \infty$$

We are interested in prescribing the worst-case L_2-gain from $\boldsymbol{u}_{\mathrm{e}} \in L_2$ to $\boldsymbol{z} \in L_2$ for all uncertain parameter values, $\boldsymbol{\theta} \in \mathbb{P}_\theta$. Thus the design goal is stated as

$$\sup_{\boldsymbol{\theta} \in \mathbb{P}_\theta} \|\boldsymbol{u}_{\mathrm{e}} \mapsto \boldsymbol{z}\|_\infty = \sup_{\mathbf{0} \neq \boldsymbol{u}_{\mathrm{e}} \in L_2,\, \boldsymbol{\theta} \in \mathbb{P}_\theta} \frac{\|\boldsymbol{z}\|_{L_2}}{\|\boldsymbol{u}_{\mathrm{e}}\|_{L_2}} = 1 \tag{29}$$

Remark 1 *The control objective stated above for system excitation is contrast with the typical robust control problem where the aim is to* suppress *disturbances. Here, we wish to create sufficiently rich "disturbances" and to only* bound *their effect on the vehicle response.*

VI. Robust LPV Control Law Design

For the control law synthesis, we consider the polytopic uncertain LPV system (23) without the position and yaw states since they are ignorable coordinates. For this system, a static state feedback control law that satisfies Eq. (29) can readily be obtained. Adapting Theorem 2 of [18] to the system in Eq. (19) for the case with no pole placement constraints or H_2 norm objectives, we have the following Lemma.

Lemma 1 (Theorem 2 in [18]) *Consider the polytopic linear, parameter-varying system with polytopic uncertainty in Eq. (19). Given a constant $\gamma > 0$, if there exist symmetric positive definite matrices $\boldsymbol{X}_i^j$, matrices $\boldsymbol{S}_i$, and a matrix $\boldsymbol{H}$*

for all $i \in \{1, \cdots, N\}$ and $j \in \{1, \cdots, M_i\}$ such that

$$\begin{bmatrix} \boldsymbol{U}_i^j + \boldsymbol{U}_i^{j\mathsf{T}} & -\boldsymbol{X}_i^j + \boldsymbol{H}^\mathsf{T} - \boldsymbol{U}_i^j & \boldsymbol{B}_{\mathrm{e}}^j & \boldsymbol{H}^\mathsf{T}\boldsymbol{C}^\mathsf{T} \\ -\boldsymbol{X}_i^j + \boldsymbol{H} - \boldsymbol{U}_i^{j\mathsf{T}} & -(\boldsymbol{H} + \boldsymbol{H}^\mathsf{T}) & \boldsymbol{0} & -\boldsymbol{H}^\mathsf{T}\boldsymbol{C}^\mathsf{T} \\ \boldsymbol{B}_{\mathrm{e}}^{j\mathsf{T}} & \boldsymbol{0} & -\mathbb{I} & \boldsymbol{0} \\ \boldsymbol{C}\boldsymbol{H} & -\boldsymbol{C}\boldsymbol{H} & \boldsymbol{0} & -\gamma^2\mathbb{I} \end{bmatrix} \prec \boldsymbol{0} \qquad (30)$$

where

$$\boldsymbol{U}_i^j = \boldsymbol{A}_i^j\boldsymbol{H} + \boldsymbol{B}_{\mathrm{c}}^j\boldsymbol{S}_i$$

then the static state feedback

$$\Delta\boldsymbol{u}_{\mathrm{c}} = \boldsymbol{K}(\boldsymbol{v}_{\mathrm{d}})\Delta\boldsymbol{x}, \qquad \boldsymbol{K}(\boldsymbol{v}_{\mathrm{d}}) = \sum_{i=1}^{N} \alpha_i(\boldsymbol{v}_{\mathrm{d}})\boldsymbol{K}_i, \qquad \boldsymbol{K}_i = \boldsymbol{S}_i\boldsymbol{H}^{-1} \qquad (31)$$

renders the H_∞ norm of the closed-system less than γ for all $\boldsymbol{v}_{\mathrm{d}} \in \mathbb{P}_{v_{\mathrm{d}}}$ and all $\boldsymbol{\theta} \in \mathbb{P}_\theta$.

Using this lemma, we can choose $\gamma = 1$ yielding a convex feasibility problem that can be solved using a linear matrix inequity (LMI) solver. If the problem is not feasible, then there are three remediations, all of which may be used. First, the input magnitudes Δ_t, Δ_a, Δ_e and Δ_r can be reduced. Second, the allowed output magnitudes Δ_u, Δ_v, and Δ_w can be increased. Third, the uncertainty in the identified LTI models can be reduced through refined model identification.

For the quadrotor model identified in Section IV, we chose the tuning parameters

$$\begin{aligned} \Delta_t = \Delta_a = \Delta_e = \Delta_r = 0.1 \\ \Delta_u = \Delta_v = \Delta_w = 5 \end{aligned} \qquad (32)$$

The convex feasibility problem in Lemma 1 was solved using CVX [19, 20] in MATLAB with the Mosek solver [21]. The total number of scalar optimization variables was 332,920 with 45,768 constraints, and the total computation time* was 52 seconds using default precision. The final result is eight feedback gain matrices that are used to compute $\boldsymbol{K}(\boldsymbol{v}_{\mathrm{d}})$ from Eq. (31). In implementation, the equilibrium state and input vectors are similarly computed as convex combinations of the vertex equilibria.

VII. Simulation

The synthesized robust LPV control law was simulated with the identified LPV model. First, the uncertain parameters were evaluated at their nominal values, $\boldsymbol{\theta}_0$, and the following closed-loop system was simulated in MATLAB using ode45:

$$\dot{\boldsymbol{x}} = \boldsymbol{A}(\boldsymbol{v}_{\mathrm{d}}, \boldsymbol{\theta}_0)(\boldsymbol{x} - \boldsymbol{x}_0) + \boldsymbol{B}_{\mathrm{c}}(\boldsymbol{\theta}_0)(\boldsymbol{u}_{\mathrm{c}} - \boldsymbol{u}_0) + \boldsymbol{B}_{\mathrm{e}}(\boldsymbol{\theta}_0)\kappa\boldsymbol{u}_{\mathrm{e}} + \dot{\boldsymbol{x}}_0 \qquad (33)$$

for some constant $\kappa > 0$. Note the designed input magnitudes of Δ_t, Δ_a, Δ_e and Δ_r need not be used, as they are just used to normalize the performance objective. If their L_2 norm is doubled, for instance, then the worst-case L_2 norm of the velocity perturbation is simply doubled as well. The important result is that we prescribe this gain. For this demonstration, however, the excitation multiplier κ was set to unity. The equilibrium state derivative, $\dot{\boldsymbol{x}}_0$, in Eq. (33) was computed with

$$\dot{\boldsymbol{x}}_0 = \frac{\partial\boldsymbol{x}_0(\boldsymbol{v}_{\mathrm{d}})}{\partial\boldsymbol{v}_{\mathrm{d}}}\frac{\mathrm{d}\boldsymbol{v}_{\mathrm{d}}}{\mathrm{d}t} \qquad (34)$$

In Figure 8, the body velocity reference is plotted in black dashed lines along with the actual body velocity in solid lines, where the time history shows sufficient tracking of the velocity reference command. The perturbation from the reference was also computed and is displayed in Figure 9. Here, the perturbations remain below an acceptable threshold and qualitatively indicate good information content.

For each axis of the nonlinear aerodynamic model given in Eq. (6), the correlation coefficients of the regressors were computed and are shown in Figure 10. Here we see good decorrelation of most regressors, indicating that we should be able accurately identify the aerodynamic parameters in Eq. (6) (assuming a sufficiently high signal-to-noise ratio, etc.). The regressors that show extremely high correlation amongst each other are those that depend on $\delta(\cdot)$. This is expected since the magnitude of excitation was small. To further decorrelate these regressors, one would set some larger $\kappa > 1$ for the final flight test experiment.

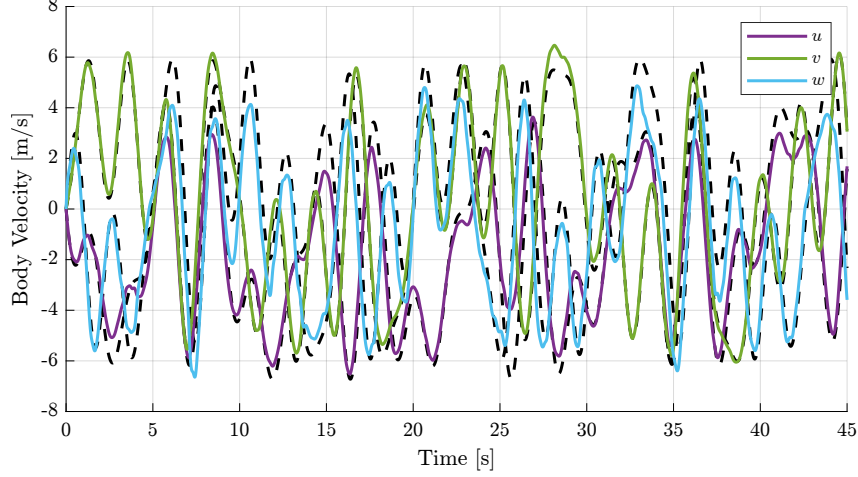*Performed on a laptop with an Intel Core i7-1185G7 and 16GB DDR4-3200 memory

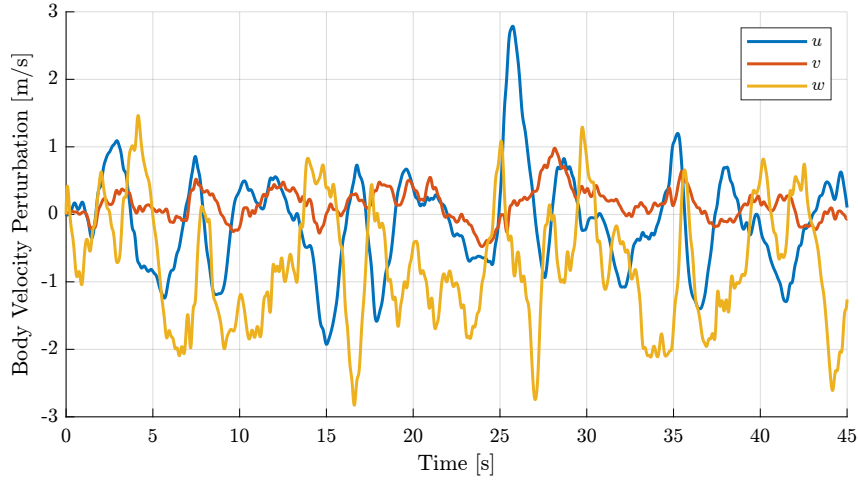**Fig. 8   Nominal model simulation body velocity and reference.**

Fig. 9   Nominal model simulation body velocity perturbation.

VIII. Conclusions and Future Work

A novel modeling methodology has been presented that supports data collection for the experimental identification of large-domain nonlinear flight dynamic models. Critically, a robust linear, parameter-varying (LPV) control result allows system excitation for unstable aircraft that is *safe* (with a user-defined bound on the input-to-state amplification) and *effective* (with sufficient excitation to identify model parameters). The method has a low barrier to implementation, requiring only an initial set of locally stabilizing control laws, such as PID controllers. With a nonlinear model postulated, initial flight data is collected that informs the identification of an LPV model for the aircraft dynamics. For a multirotor, we have shown this step involves only eight maneuvers, each corresponding to a body velocity reference condition. The next step of this process consists of excitation and reference signal design and control law synthesis via a linear matrix inequality. For the multirotor, a 7-axis multisine signal is designed to ensure the body velocity reference is uncorrelated from the actuator commands. The convex feasibility problem is readily solved, yielding a parameter-varying state-feedback robust H_∞ control law. Finally, the second phase of data collection is conducted using the robust LPV control law in order to obtain rich data over the entire flight envelope. At the time of publication, a flight test program was being developed to implement the procedure on the aircraft shown in Figure 1.
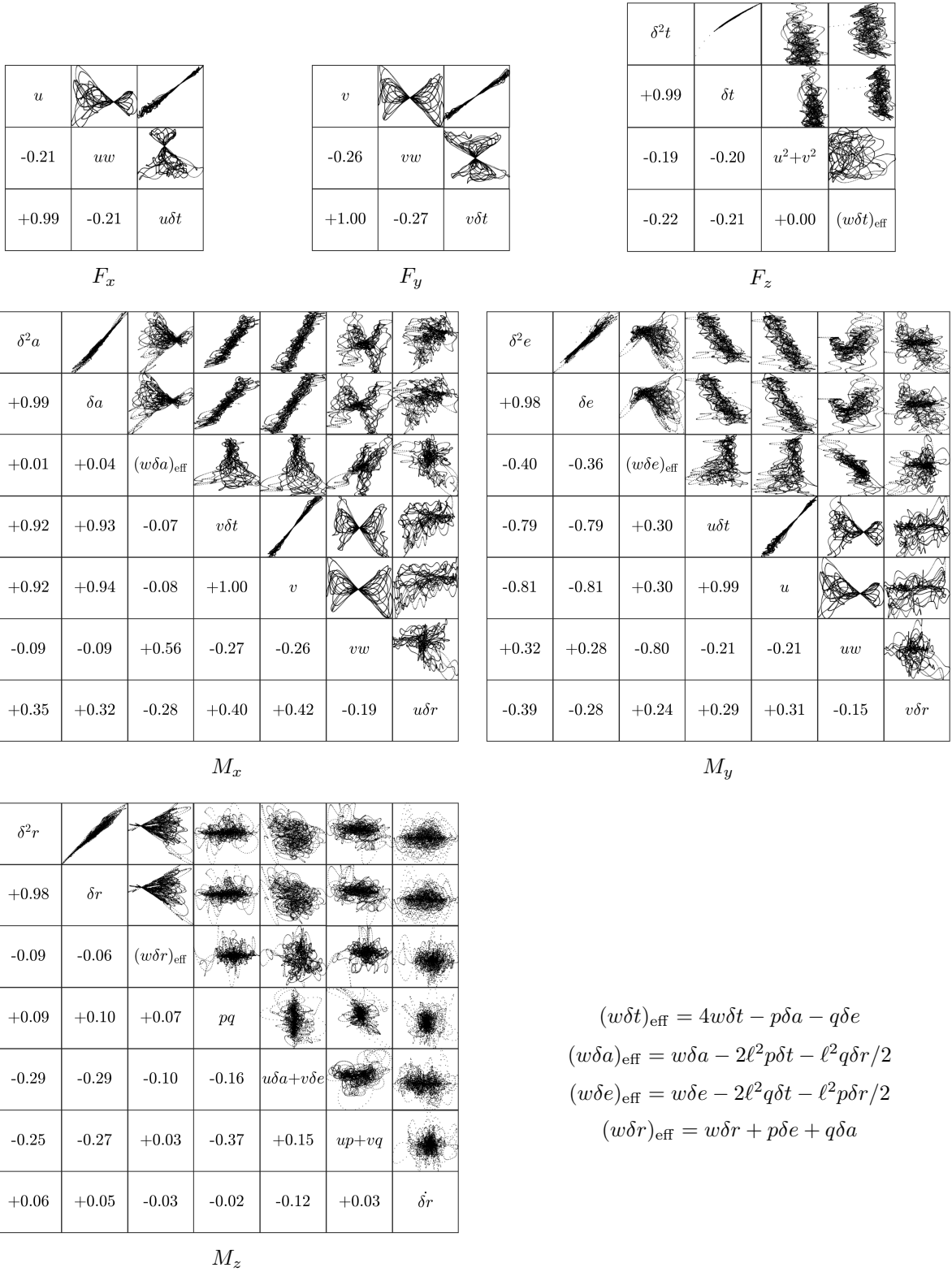
F_x

F_y

F_z

M_x

M_y

M_z

$$(w\delta t)_{\text{eff}} = 4w\delta t - p\delta a - q\delta e$$
$$(w\delta a)_{\text{eff}} = w\delta a - 2\ell^2 p\delta t - \ell^2 q\delta r/2$$
$$(w\delta e)_{\text{eff}} = w\delta e - 2\ell^2 q\delta t - \ell^2 p\delta r/2$$
$$(w\delta r)_{\text{eff}} = w\delta r + p\delta e + q\delta a$$

Fig. 10   Nonlinear model regressor correlation.

A. Quadrotor LPV Aerodynamic Model Structure

The elements of the matrices $\mathcal{A}_{(\cdot)}$ and $\mathcal{B}_{(\cdot)}$ from Eq. (12) that are functions of the unknown parameter vector, $\boldsymbol{\vartheta}$, are indicated with a "$\bullet$" as follows.

$$\mathcal{A}_0 = \begin{bmatrix} \bullet & 0 & 0 & 0 & 0 & 0 \\ 0 & \bullet & 0 & 0 & 0 & 0 \\ 0 & 0 & \bullet & 0 & 0 & 0 \\ 0 & \bullet & 0 & \bullet & 0 & 0 \\ \bullet & 0 & 0 & 0 & \bullet & 0 \\ 0 & 0 & 0 & 0 & 0 & 0 \end{bmatrix} \qquad \mathcal{A}_u = \begin{bmatrix} \bullet & 0 & \bullet & 0 & 0 & 0 \\ 0 & \bullet & 0 & 0 & 0 & 0 \\ \bullet & 0 & \bullet & \bullet & \bullet & 0 \\ \bullet & \bullet & \bullet & \bullet & \bullet & 0 \\ \bullet & \bullet & \bullet & \bullet & \bullet & 0 \\ \bullet & \bullet & \bullet & \bullet & \bullet & 0 \end{bmatrix}$$

$$\mathcal{A}_v = \begin{bmatrix} \bullet & 0 & 0 & 0 & 0 & 0 \\ 0 & \bullet & \bullet & 0 & 0 & 0 \\ 0 & \bullet & \bullet & \bullet & \bullet & 0 \\ \bullet & \bullet & \bullet & \bullet & \bullet & 0 \\ \bullet & \bullet & \bullet & \bullet & \bullet & 0 \\ \bullet & \bullet & \bullet & \bullet & \bullet & 0 \end{bmatrix} \qquad \mathcal{A}_w = \begin{bmatrix} \bullet & 0 & 0 & 0 & 0 & 0 \\ 0 & \bullet & 0 & 0 & 0 & 0 \\ 0 & 0 & \bullet & \bullet & \bullet & 0 \\ \bullet & \bullet & \bullet & \bullet & \bullet & 0 \\ \bullet & \bullet & \bullet & \bullet & \bullet & 0 \\ \bullet & \bullet & \bullet & \bullet & \bullet & 0 \end{bmatrix}$$

$$\mathcal{B}_0 = \begin{bmatrix} 0 & 0 & 0 & 0 \\ 0 & 0 & 0 & 0 \\ \bullet & 0 & 0 & 0 \\ 0 & \bullet & 0 & 0 \\ 0 & 0 & \bullet & 0 \\ 0 & 0 & 0 & \bullet \end{bmatrix} \quad \mathcal{B}_u = \begin{bmatrix} \bullet & 0 & 0 & 0 \\ 0 & 0 & 0 & 0 \\ \bullet & \bullet & \bullet & \bullet \\ \bullet & \bullet & \bullet & \bullet \\ \bullet & \bullet & \bullet & \bullet \\ \bullet & \bullet & \bullet & \bullet \end{bmatrix} \quad \mathcal{B}_v = \begin{bmatrix} 0 & 0 & 0 & 0 \\ \bullet & 0 & 0 & 0 \\ \bullet & \bullet & \bullet & \bullet \\ \bullet & \bullet & \bullet & \bullet \\ \bullet & \bullet & \bullet & \bullet \\ \bullet & \bullet & \bullet & \bullet \end{bmatrix} \quad \mathcal{B}_w = \begin{bmatrix} 0 & 0 & 0 & 0 \\ 0 & 0 & 0 & 0 \\ \bullet & \bullet & \bullet & \bullet \\ \bullet & \bullet & \bullet & \bullet \\ \bullet & \bullet & \bullet & \bullet \\ \bullet & \bullet & \bullet & \bullet \end{bmatrix}$$

B. Equation-Error Grey-Box Identification

Consider the linear, time-invariant state equation

$$\dot{\boldsymbol{x}} = \boldsymbol{A}\boldsymbol{x} + \boldsymbol{B}\boldsymbol{u} \tag{35}$$

where the elements of $\boldsymbol{A}$ and $\boldsymbol{B}$ depend on both known constants (e.g. gravitational acceleration) and unknown parameters (e.g. aerodynamic coefficients). Let $\boldsymbol{x} = [x_1 \; \cdots \; x_{n_x}]^\mathsf{T}$ and $\boldsymbol{u} = [u_1 \; \cdots \; u_{n_u}]^\mathsf{T}$. Define the index sets

$$\mathcal{I}_A = \{(i,j) \mid A_{ij} \text{ unknown}, \; i,j = 1, \cdots, n_x\} \tag{36}$$

$$\mathcal{I}_B = \{(i,j) \mid B_{ij} \text{ unknown}, \; i = 1, \cdots, n_x, \; j = 1, \cdots, n_u\} \tag{37}$$

and their "complements"

$$\overline{\mathcal{I}}_A = \{(i,j) \mid A_{ij} \text{ known}, \; i,j = 1, \cdots, n_x\} \tag{38}$$

$$\overline{\mathcal{I}}_B = \{(i,j) \mid B_{ij} \text{ known}, \; i = 1, \cdots, n_x, \; j = 1, \cdots, n_u\} \tag{39}$$

Let the row vector of regressors for the ith row of the state equation be defined as

$$\boldsymbol{h}_i = \begin{bmatrix} \boldsymbol{x}_j^\mathsf{T} & \boldsymbol{u}_k^\mathsf{T} \end{bmatrix}, \quad (i,j) \in \mathcal{I}_A, \quad (i,k) \in \mathcal{I}_B \tag{40}$$

where for each i, $\boldsymbol{x}_j$ and $\boldsymbol{u}_k$ are column vectors containing the components of $\boldsymbol{x}$ and $\boldsymbol{u}$ defined by the index sets $\mathcal{I}_A$ and $\mathcal{I}_B$. Then, let the measurement for the ith row of the state equation be

$$y_i = \dot{x}_i - \sum_j A_{ij} x_j - \sum_k B_{ik} u_k, \quad (i,j) \in \overline{\mathcal{I}}_A, \quad (i,k) \in \overline{\mathcal{I}}_B \tag{41}$$

For each row of the state equation, define the column vector of parameters

$$\boldsymbol{\theta}^{(i)} = \begin{bmatrix} \boldsymbol{A}_j^{\mathsf{T}} \\ \boldsymbol{B}_k^{\mathsf{T}} \end{bmatrix}, \quad (i,j) \in \mathcal{I}_A, \quad (i,k) \in \mathcal{I}_B \tag{42}$$

where for each i, $\boldsymbol{A}_j$ and $\boldsymbol{B}_k$ are constructed from the elements of the ith rows of $\boldsymbol{A}$ and $\boldsymbol{B}$ according to the index sets $\mathcal{I}_A$ and $\mathcal{I}_B$, respectively. *Note: The preceding derivation and notation is presented for easy implementation in MATLAB.*

With these definitions, a sample has the model

$$y_i = \boldsymbol{h}_i \boldsymbol{\theta}^{(i)}, \quad i = 1, \cdots, n_x \tag{43}$$

for each $i = 1, \cdots, n_x$. Now suppose we take K samples of y_i and $\boldsymbol{h}_i$, where the kth sample is denoted $y_i(k)$, $\boldsymbol{x}(k)$, and $\boldsymbol{u}(k)$, etc. Let the measurements be subjected to additive, white, Gaussian noise such that

$$z_i(k) = y_i(k) + w_i(k), \quad k = 1, \cdots, K, \quad i = 1, \cdots, n_x \tag{44}$$

Stacking the K measurements and regressors, we obtain

$$\boldsymbol{y}_i = \begin{bmatrix} y_i(1) \\ y_i(2) \\ \vdots \\ y_i(K) \end{bmatrix}, \qquad \boldsymbol{H}_i = \begin{bmatrix} \boldsymbol{h}_i(1) \\ \boldsymbol{h}_i(2) \\ \vdots \\ \boldsymbol{h}_i(K) \end{bmatrix}, \qquad \text{and} \qquad \boldsymbol{w}_i = \begin{bmatrix} w_i(1) \\ w_i(2) \\ \vdots \\ w_i(K) \end{bmatrix} \tag{45}$$

Then, the measurement equations are

$$\boldsymbol{y}_i = \boldsymbol{H}_i \boldsymbol{\theta}^{(i)}, \quad i = 1, \cdots, n_x \tag{46}$$

from which one obtains the least square error parameter estimates

$$\boldsymbol{\theta}^{(i)} = (\boldsymbol{H}_i^{\mathsf{T}} \boldsymbol{H}_i)^{-1} \boldsymbol{H}_i^{\mathsf{T}} \boldsymbol{y}_i, \quad i = 1, \cdots, n_x \tag{47}$$

References

[1] Morelli, E., "Efficient Global Aerodynamic Modeling from Flight Data," *50th AIAA Aerospace Sciences Meeting Including the New Horizons Forum and Aerospace Exposition*, American Institute of Aeronautics and Astronautics, Nashville, Tennessee, 2012, pp. 1–26. https://doi.org/10.2514/6.2012-1050.

[2] Grauer, J. A., and Morelli, E. A., "Generic Global Aerodynamic Model for Aircraft," *Journal of Aircraft*, Vol. 52, No. 1, 2015, pp. 13–20. https://doi.org/10.2514/1.C032888.

[3] Van Den Hof, P. M., and Schrama, R. J., "Identification and Control — Closed-loop Issues," *Automatica*, Vol. 31, No. 12, 1995, pp. 1751–1770. https://doi.org/10.1016/0005-1098(95)00094-X.

[4] Jategaonkar, R. V., *Flight Vehicle System Identification: A Time-Domain Methodology*, 2nd ed., Progress in Astronautics and Aeronautics, American Institute of Aeronautics and Astronautics, Inc., Reston, Virginia, 2015.

[5] Morelli, E. A., and Klein, V., *Aircraft System Identification: Theory and Practice*, 2nd ed., Sunflyte Enterprises, Williamsburg, Virginia, 2016.

[6] Cunningham, M. A., and Hubbard, J. E., "Open-Loop Linear Model Identification of a Multirotor Vehicle with Active Feedback Control," *Journal of Aircraft*, Vol. 57, No. 6, 2020, pp. 1044–1061. https://doi.org/10.2514/1.C035834.

[7] Cooper, J., Hopwood, J. W., Woolsey, C. A., De Wekker, S. F. J., and DeVore, M., "Intelligent Wind Estimation for Chemical Source Localization," *79th Annual Forum & Technology Display*, Vertical Flight Society, West Palm Beach, FL, 2023, pp. 1–20. https://doi.org/10.4050/F-0079-2023-18194.

[8] Simmons, B. M., McClelland, H. G., and Woolsey, C. A., "Nonlinear Model Identification Methodology for Small, Fixed-Wing, Unmanned Aircraft," *Journal of Aircraft*, Vol. 56, No. 3, 2019, pp. 1056–1067. https://doi.org/10.2514/1.C035160.

[9] Gresham, J. L., Fahmi, J.-M. W., Simmons, B. M., Hopwood, J. W., Foster, W., and Woolsey, C. A., "Flight Test Approach for Modeling and Control Law Validation for Unmanned Aircraft," *AIAA SCITECH 2022 Forum*, American Institute of Aeronautics and Astronautics, San Diego, CA & Virtual, 2022, pp. 1–23. https://doi.org/10.2514/6.2022-2406.

[10] Simmons, B. M., Gresham, J. L., and Woolsey, C. A., "Flight-Test System Identification Techniques and Applications for Small, Low-Cost, Fixed-Wing Aircraft," *Journal of Aircraft*, Vol. 60, No. 5, 2023, pp. 1503–1521. https://doi.org/10.2514/1.C037260.

[11] Hopwood, J. W., Simmons, B. M., and Woolsey, C. A., "Multirotor Flight Dynamic Models and Experiment Design for Estimation and Control," *AIAA SCITECH 2024 Forum*, American Institute of Aeronautics and Astronautics, Kissimmee, Florida, 2024, p. To appear.

[12] Szafranski, G., Czyba, R., and Blachuta, M., "Modeling and Identification of Electric Propulsion System for Multirotor Unmanned Aerial Vehicle Design," *2014 International Conference on Unmanned Aircraft Systems (ICUAS)*, IEEE, Orlando, FL, USA, 2014, pp. 470–476. https://doi.org/10.1109/ICUAS.2014.6842287.

[13] Gahinet, P., Nemirovski, A., Laub, A. J., and Chilali, M., "LMI Control Toolbox User's Guide," , May 1995.

[14] Morelli, E. A., "System IDentification Programs for AirCraft (SIDPAC), Version 4.0," NASA Langley Research Center, 2018.

[15] Morelli, E. A., "Practical Aspects of Multiple-Input Design for Aircraft System Identification Flight Tests," *AIAA AVIATION 2021 FORUM*, American Institute of Aeronautics and Astronautics, VIRTUAL EVENT, 2021, pp. 1–25. https://doi.org/10.2514/6.2021-2795.

[16] Simmons, B. M., Gresham, J. L., and Woolsey, C. A., "Aero-Propulsive Modeling for Propeller Aircraft Using Flight Data," *Journal of Aircraft*, Vol. 60, No. 1, 2023, pp. 81–96. https://doi.org/10.2514/1.C036773.

[17] Ivler, C. M., Rowe, E. S., Martin, J., Lopez, M. J., and Tischler, M. B., "System Identification Guidance for Multirotor Aircraft: Dynamic Scaling and Test Techniques," *Journal of the American Helicopter Society*, 2021. https://doi.org/10.4050/JAHS.66.022006.

[18] Rotondo, D., Nejjari, F., and Puig, V., "Robust State-Feedback Control of Uncertain LPV Systems: An LMI-based Approach," *Journal of the Franklin Institute*, Vol. 351, No. 5, 2014, pp. 2781–2803. https://doi.org/10.1016/j.jfranklin.2014.01.018.

[19] Grant, M., and Boyd, S., "CVX: Matlab Software for Disciplined Convex Programming, Version 2.1," , Mar. 2014.

[20] Grant, M. C., and Boyd, S. P., "Graph Implementations for Nonsmooth Convex Programs," *Recent Advances in Learning and Control*, Vol. 371, edited by V. D. Blondel, S. P. Boyd, and H. Kimura, Springer London, London, 2008, pp. 95–110. https://doi.org/10.1007/978-1-84800-155-8_7.

[21] ApS, M., "The MOSEK Optimization Toolbox for MATLAB Manual," , 2022.